Photonic crystal carpet: Manipulating wave fronts in the near field at 1.55 μm

Geoffroy Scherrer, Maxence Hofman, Wojciech Smigaj, Muamer Kadic, T.M. Chang, Xavier Mélique, D. Lippens, Olivier Vanbésien, Benoit Cluzel, Frederique de Fornel, et al.

Photonic crystal carpet: Manipulating wave fronts in the near field at 1.55 μm

G. Scherrer,[1] M. Hofman,[2] W. Śmigaj,[3,4] M. Kadic,[5] T.-M. Chang,[5] X. Mélique,[2] D. Lippens,[2] O. Vanbésien,[2] B. Cluzel,[1] F. de Fornel,[1] S. Guenneau,[5] and B. Gralak[5]

[1]*OCP–ICB, UMR CNRS 6303, 9 Avenue A. Savary, BP 47870, 21078 Dijon, France*

[2]*IEMN, UMR CNRS 8520, Université Lille 1, BP 60069, 59652 Villeneuve d'Ascq Cedex, France*

[3]*Department of Mathematics, University College London, Gower Street, London WC1E 6BT, United Kingdom*

[4]*Faculty of Physics, Adam Mickiewicz University, Umultowska 85, 61-614 Poznań, Poland*

[5]*Aix-Marseille Université, CNRS, Ecole Centrale Marseille, Institut Fresnel, 13013 Marseille, France*

(Received 19 July 2012; revised manuscript received 4 July 2013; published 6 September 2013)

Ground-plane cloaks, which transform a curved mirror into a flat one, and recently reported at wavelengths ranging from the optical to the visible spectrum, bring the realm of optical illusion a step closer to reality. However, all carpet-cloaking experiments have thus far been carried out in the far field. Here, we demonstrate numerically and experimentally that a dielectric photonic crystal (PC) of an irregular shape made of a honeycomb array of air holes can scatter waves in the near field like a PC with a flat boundary at stop band frequencies. This mirage effect relies upon a specific arrangement of dielectric pillars placed at the nodes of a quasiconformal grid dressing the PC. Our carpet is experimentally shown to flatten the scattered wave fronts of a PC with a bump throughout the range of wavelengths from 1520 to 1580 nm within the stop band extending from 1280 to 1940 nm. The device has been fabricated using a single-mask advanced nanoelectronics technique on III-V semiconductors and the near field measurements have been carried out in order to image the wave fronts' curvatures around the telecommunication wavelength 1550 nm. Interestingly, comparisons of our near-field experimental results with full-wave simulations suggest the relatively low aspect ratio of the fabricated carpet (pillars have 200 nm diameter and 2 μm height) makes it inherently three dimensional. Moreover, this carpet is constrained to normal incidence. We therefore propose an elaborated design of the carpet (with pillars of varying radii) which should work at different angles of incidence.

DOI: 10.1103/PhysRevB.88.115110 PACS number(s): 42.79.Ry, 07.79.Fc, 42.30.Rx, 42.82.Cr

I. INTRODUCTION

The current interest in a better control of light through transformational optics can be linked to the pioneering theoretical works of Pendry *et al.*[1] and Leonhardt[2] published in 2006. The former seminal paper demonstrates the possibility of designing a cloak that renders any object inside it invisible to electromagnetic radiation (using the covariant structure of Maxwell's equations)[3], while the latter concentrates on the ray-optics limit (using conformal mappings in the complex plane). In both cases, the cloak consists of a metamaterial whose physical properties (permittivity and permeability) are spatially varying and matrix-valued. These theoretical considerations might have remained an academic curiosity without the experimental validation in 2006 (Ref. 4) of an electromagnetic cloak making a copper cylinder invisible to an incident plane wave at 8.5 GHz. This demonstration immediately sparked a widespread interest in the optical community with the fabrication and characterization of a similar nonmagnetic cloak for microwaves.[5]

It must be noted that the originally proposed invisibility cloak suffers from an inherent narrow bandwidth as its transformational optics (TO) design leads to singular (i.e., infinitely anisotropic) permittivity and permeability tensors on the boundary of the invisibility region. This is due to the fact that this invisibility region is created by the blow-up of a point in order to hide an object in the resulting metric hole. This TO approach to cloaking therefore requires extreme material parameters, which can only be achieved with resonant structures. This route to invisibility is reminiscent of the work of Greenleaf *et al.* in the context of electrical impedance tomography.[6] Interestingly, Leonhardt and Tyc[7] have extended TO to non-Euclidean spaces, making use of the stereographic projection of a higher-dimensional sphere onto the space where the cloak needs to be constructed. In this way, superluminal issues can be avoided.[8] Other proposals of cloak singularity removal include blowing up a small ball[9] or a segment[10] instead of a point, but these remain theoretical proposals to this date.

However, the carpet-cloaking scheme proposed by Li and Pendry in 2008 (Ref. 11) circumvents all these issues, since its TO design is based upon an easily implementable one-to-one map (a curved surface is transformed into a flat surface). In layman terms, the philosophy of this renewed approach to cloaking is to sweep dust under a bump in a carpet. The challenge is that the bump should not be detected either by an external observer. One possible way to achieve this trick is to make a very small bump, but this would have limited interest for applications.[12] The bold idea of Li and Pendry was to choose instead to create a mirage effect by curving wave trajectories around the bump so that the carpet would appear to be flat to an external observer. Since then, carpet cloaking has fuelled the experimental realization of cloaks at microwave, terahertz, near-infrared, and even visible frequencies,[13–18] including a carpet hiding a macroscopic object in the visible spectrum.[19]

Herein, we propose to mimic the optical response of a flat mirror by a photonic crystal (PC) of irregular shape for wavelengths lying in its band gap. This optical illusion is achieved using dielectric pillars with subwavelength diameter. The ability of reconstructing the wave fronts in the vicinity of the carpet is shown using near-field scanning optical microscopy (NSOM).[20] At optical frequencies, the previous

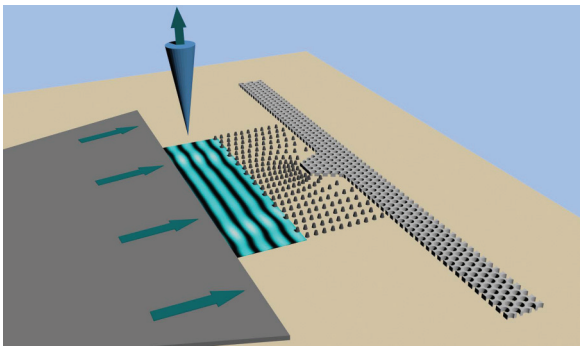

FIG. 1. (Color online) Experimental setup (from right to left): Flat mirror with a bump of trapezoidal shape made of holes arranged along a periodic array; surrounding carpet made of pillars; injection guide generating an incident plane wave. Above the structure, probe measuring the near field.

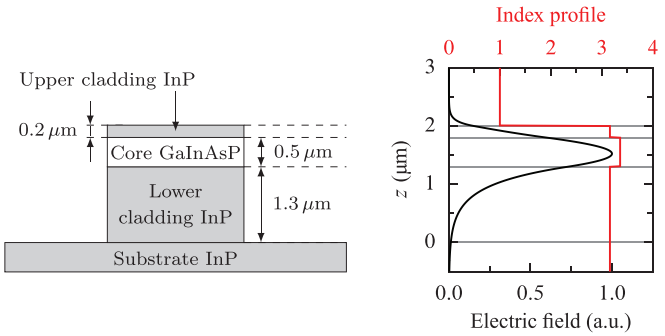

FIG. 2. (Color online) Left: Epitaxial sequence of the guiding heterostructure. Right: Index profile and supported p-fundamental mode in the vertical direction (the magnetic field is oriented along the vertical z axis).

TO-based carpet cloaks were demonstrated by far-field microscopy methods[13–16] or leakage radiation microscopy.[17] Those techniques are not suitable for our experimental setup described in Fig. 1. In this configuration, light successively propagates through free space and guiding areas over large distances (more than 10 μm between the very end of the injection guide and the input interface of the flat mirror). Thus, far-field microscopy would mainly allow access to scattered light such as out-of-plane losses, and leakage radiation microscopy would not be appropriate to measure wave fronts in the free space area. Such disadvantages clearly disappear with a near-field technique. NSOM provides a direct local probing of the electric field with a high spatial resolution, notably thanks to the piezoelectric scanners associated with the probe. This markedly enhances our capabilities to manipulate light, even in the extreme near field limit, when a source lies a fraction of wavelength from the carpet cloak.[21] The phase control, as shown by NSOM measurements, may find important applications in integrated optics for impedance matching[22–24] and for devices like microprisms[25,26] and microlenses.[22,23,26]

The plan of the paper is as follows. We first describe a PC which is used to mimic a mirror and to realize the reference structure. A trapezoidal bump on one side of this PC plays the role of the object to hide. Then, a pillar structure designed using a quasiconformal mapping is proposed to cloak the PC bump. Numerical simulations have been performed to show the efficiency of the design for wavelengths ranging from 1500 to 1650 nm. These composite structures consisting of a combination of air holes and dielectric pillars have been fabricated with a one-mask process. Next, near field measurements demonstrate the ability of the carpet to hide the bump in the near field at frequencies around the telecommunication wavelength 1550 nm. The study at normal incidence is completed with an analysis based on 3D simulations. Finally, another 2D carpet is designed and shown numerically to operate for different angles of incidence.

II. DESIGN OF A PHOTONIC CRYSTAL CARPET CLOAK FOR NORMAL INCIDENCE

The first step is to consider a PC consisting of air holes in a dielectric matrix to build an efficient mirror at optical wavelengths. In view of the fabrication, the guiding structure defined in Ref. 27 is considered (see Fig. 2, left panel). It is made of an InGaAsP guiding layer with thickness 500 nm and index 3.36, sandwiched between a 200-nm-thick layer of InP with index 3.16 and a substrate consisting of the same material. For the sake of simplicity, this multilayer is modelled by an effective medium of index 3.26, corresponding to the effective index of the fundamental p mode of this heterostructure (Fig. 2, right panel). As shown in Fig. 3, introduction of a hexagonal lattice of air holes of diameter $d = 347$ nm and period $a = 470$ nm into this homogeneous medium leads to the formation of a p-polarization band gap for wavelengths λ ranging from 1280 to 1940 nm, i.e., for a/λ from 0.242 to 0.369.

An additional challenge compared to a metallic mirror is the variation of the phase of the reflection coefficient within the band gap. Indeed, compared to ground carpet cloaks designed for curved metal surfaces, where the boundary condition is of the Dirichlet or Neumann type depending upon light's polarization, a carpet cloak on a dielectric half space[28] requires greater care, since the mathematical model now involves (anisotropic) transmission conditions at the interface between the carpet and the dielectric half space (which in our case consists of a PC). In Fig. 4, the phase of reflection coefficient at normal incidence (upper panel) is shown to vary monotonically from $-\pi$ to zero across the stop band. The resulting dispersion will have an adverse effect on broadband cloaking. More particularly, it is noted that, at the telecommunication wavelength corresponding to

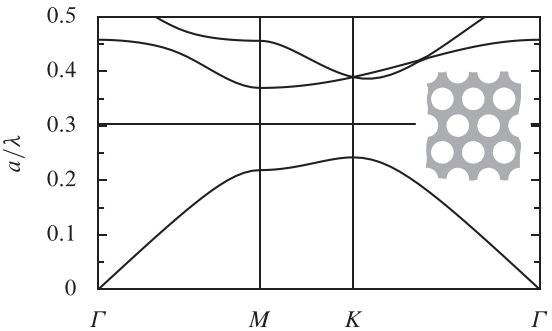

FIG. 3. The band structure of the photonic crystal for the p polarization. The telecommunication wavelength 1.55 μm corresponds to $a/\lambda = 0.303$ (marked by the horizontal line).

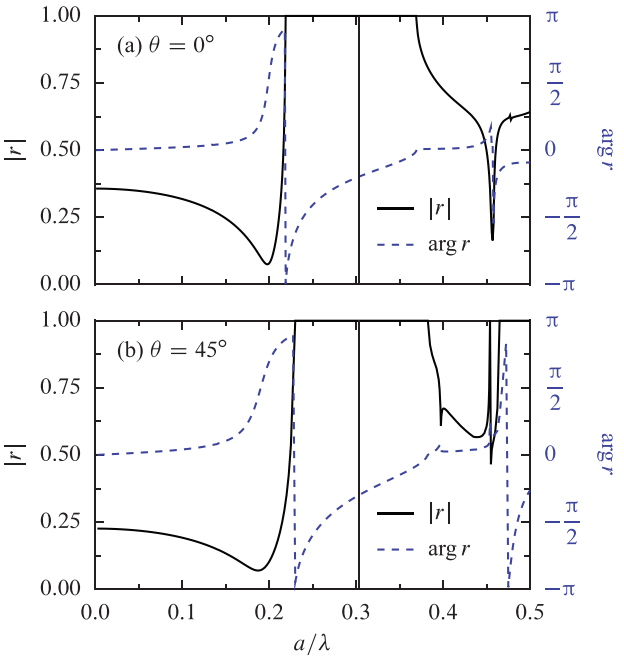

FIG. 4. (Color online) Variation of the reflection coefficient of the photonic crystal at normal incidence (upper panel) and at the incidence angle of 45 degrees (lower panel) incidence. It is noted that within the stop band r has unit magnitude (solid curves), but its phase varies monotonically from $-\pi$ to 0 (dashed curves).

$a/\lambda = 0.303$, the phase $\arg(r) = -35^\circ$ of the PC is much different from the π phase shift of a mirror, which is only achieved at the lower edge of the stop band. Moreover, the reflection depends upon the angle of incidence. Notably, at the incidence angle $\theta = 45^\circ$ the interval of a/λ for which $|r| = 1$ is slightly shifted towards shorter wavelengths and the phase at the telecommunication wavelength corresponding to $a/\lambda = 0.303$ is now $\arg(r) = -54^\circ$, as shown in the lower panel of Fig. 4. This makes the design of a carpet working for different frequencies and angles of incidence more complicated.

The goal of carpet cloaking is to hide the bump of a trapezoidal shape as shown in Fig. 1 using a heterogeneous metamaterial (a medium with a subwavelength structure). In the present case, we opted for a carpet made of dielectric pillars. For this we build a quasiconformal grid deduced from conformal-optics considerations:[11,13,15–18] This approach preserves the isotropy of the medium, unlike conventional TO tools used for cloaking.[1] We then place cylinders of diameter 200 nm at the nodes of the transformed grid. We importantly note that the minimization of the modified Liao functional,[29] which is usually invoked in recent papers on the carpet cloaking, can be replaced by a computation of potential. In other words, we build a conformal grid which preserves the right angles. If one can set up an electrostatic problem where the vertical lines are the electric field lines, then one can easily compute the equipotentials which are orthogonal at each point. The index distribution is then obtained numerically for each elementary cell of the grid using a simple vector product.[11] The structure is then built by placing the dielectric pillars at the nodes of the conformal grid. We note that this approach has been successfully used for the design of a broadband plasmonic carpet[18] and it is reminiscent of the work of Liang and Li,[30] where Bloch waves follow curved trajectories in transformed photonic crystals. The air holes in the PC and the dielectric pillars in the carpet have comparable diameters, hence the pillars are not deeply subwavelength in the stop band. Our PC carpet can therefore be considered as an intermediate configuration between a transformed PC (Bragg regime) and a conformal metamaterial (homogenization regime), keeping in mind artificial anisotropy is unwanted here.

III. FABRICATION

The device is fabricated using advanced nanoelectronics techniques on III–V semiconductors. We start from an InP-based heterostructure (InP–200 nm/InGaAsP–500 nm/InP–1300 nm) grown by molecular beam epitaxy to confine light (at 1.55 μm) in the vertical direction. To create the two-dimensional patterning, we take benefit of the one-mask process primarily developed for PC based flat lenses.[27] In brief, we employ a negative resist (HSQ) mask used for the electron beam lithography step to define simultaneously the matrix of the reflector, the pillars of the cloaking area, as well as the injection guide constituted here of a monomode ridge waveguide progressively enlarged to form the quasiplane wave requested to illuminate the device. After development and a densification by an O_2 plasma of the HSQ resist, the mask pattern is preserved for the inductively coupled plasma (ICP) etching step. The fabricated device, shown in Fig. 5, confirms that the process is able to achieve in one step 200 nm diameter pillars even in close proximity (separation less than 50 nm in front of the reflector) and a PC with a period of 470 nm and 347 nm hole diameter over a depth larger than 1.5 μm. The highly anisotropic character of the etching is preserved, which permits us to reproduce with a high degree of accuracy the theoretical dimensions targeted.

The etching depth, larger than 1.5 μm, plays a vital role. For our combined hole/pillar device, etching kinetics depends on the local environment due to species evacuation. Etching velocity is significantly lower in hole areas than in pillar regions. The process has been optimized to reach hole depths of about 1.5 μm,[31] leading to pillar heights between 2 and 2.2 μm.

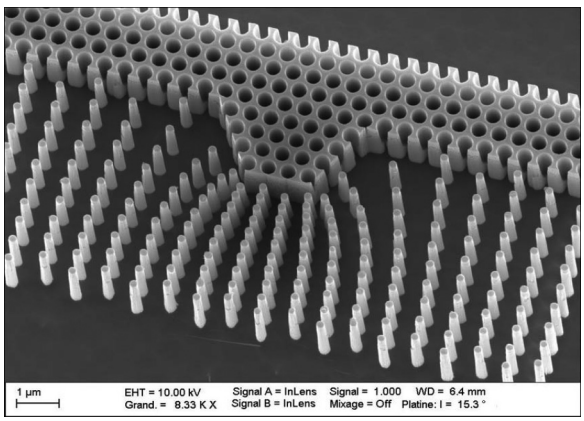

FIG. 5. SEM (scanning electron microscope) picture of the InP-based fabricated device operating at 1.55 μm: PC reflector (period 470 nm, hole diameter 347 nm) and dielectric PC carpet (pillars have diameter 200 nm and height 2 μm).

Both values are sufficient to ensure that the integrated device works in a regime which can be accurately modelled by a two-dimensional system since most of the electromagnetic energy of the guided mode will be controlled by the etching, as demonstrated in Fig. 2. In addition, it can be expected from Fig. 2 that the out-of-plane losses are moderate enough to observe the effect of the carpet, an assumption which will be experimentally validated in the sequel. This large etching depth is a key point of our fabrication process which combines holes and pillars: This yields high quality results for the field measurements.

IV. MEASUREMENTS

The concept is verified in Fig. 6 using NSOM in collection mode.[27] Thanks to the configuration of both devices and experimental set up, a phase imaging is performed by a unique near field intensity measure without optical heterodyne detection.[20] The measurement of the reflection on a flat photonic crystal (upper panel) is similar to the lower panel (cloaked bump). We can see an improvement in the alignment of the scattered wave fronts compared to the bump taken on its own in the middle panel, see also Fig. 7.

Before considering the optical images, it is important to note that the deep etching of the structures leads to large vertical displacements of the probe during the near-field scans, which may affect the formation of the optical images. However, despite this strongly modulated topology, the submicrometric features of the samples are properly resolved in all cases, which is particularly challenging for the sharp pillars of the cloak as

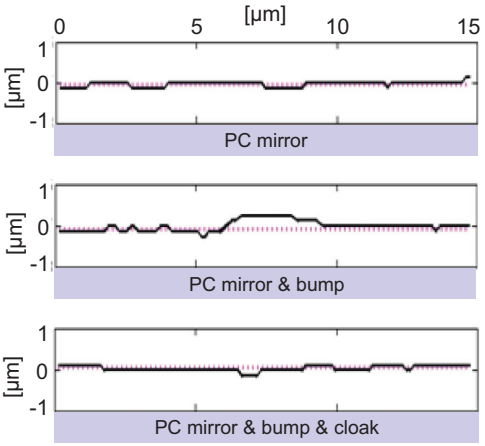

FIG. 7. (Color online) Curves following the maxima of the field intensity for the mirror (top), the mirror with bump (middle), and the cloaked structure (bottom). The resulting reduction of the bump signature is 4.75 (computed using the blue curve in the upper panel as a benchmark, and comparing its area against that of the blue curves in the middle and lower panels).

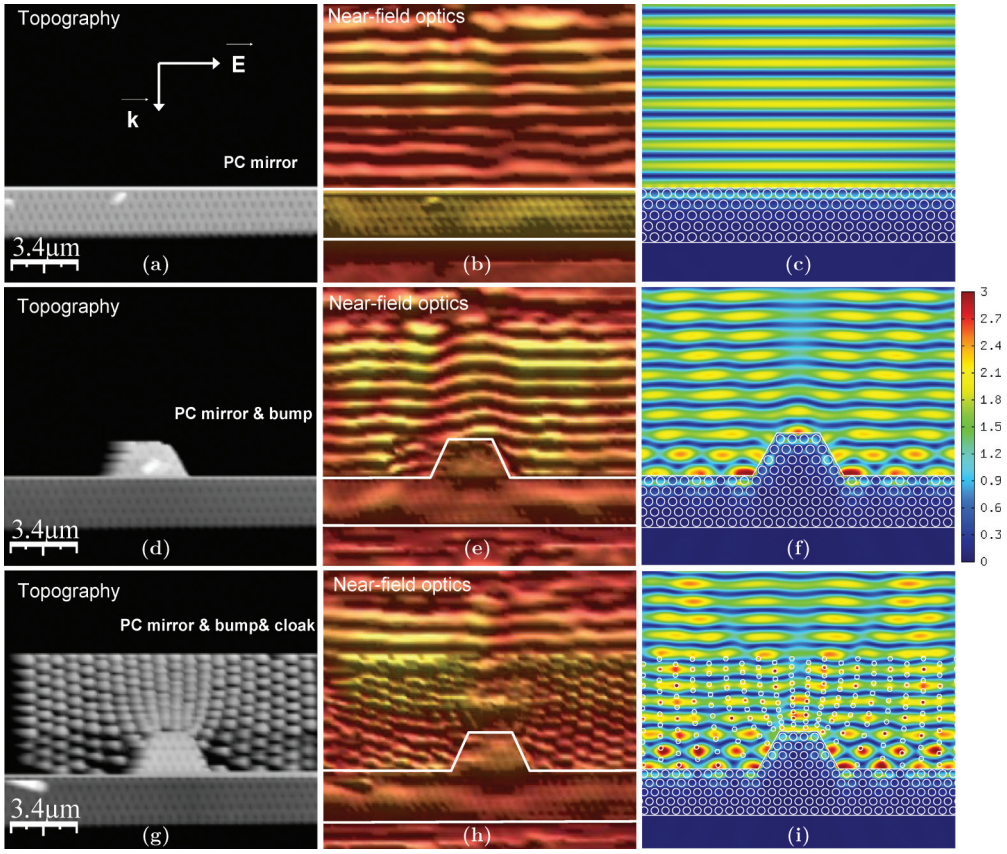

FIG. 6. (Color online) Left column: Top view of the topographical images recorded by NSOM above the two reference structures, the flat mirror (a) and the mirror with bump (d), and above the cloaked structure (g). Central column: Corresponding optical near-field intensity images recorded for a 1540 nm wavelength. Right column: Numerical simulations for the amplitude of the field (the amplitude of the incident plane wave is set to unity).

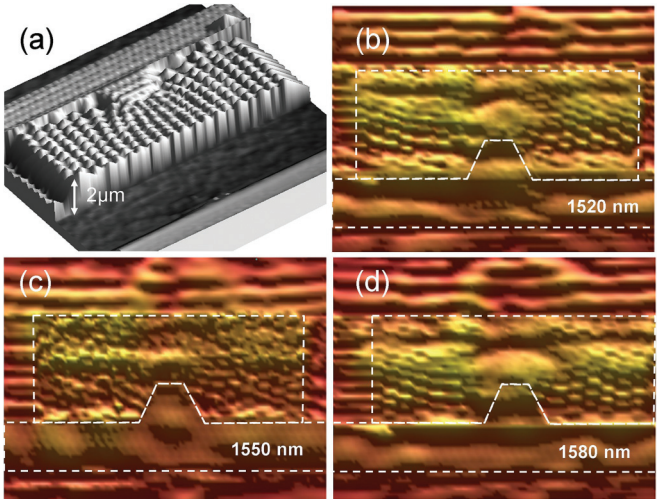

FIG. 8. (Color online) Three dimensional view (a) of topographical images of the cloak, bump, and mirror recorded in near field by NSOM. Corresponding near-field optical images recorded at (b) 1520, (c) 1550, and (d) 1580 nm.

well as for the photonic crystal mirrors. A three-dimensional view of the measured topography is provided for illustrative purposes in Fig. 8(a).

The optical images, shown in Fig. 6, present the typical optical behavior of the different structures at a telecommunication wavelength of 1540 nm. A standard illuminated view of the optical images is chosen here because of a lateral modulation of the intensity of the plane wave impinging on the structure. This can be attributed to a nonadiabatic tapering of the input waveguides. However, as shown hereafter, this is not an issue for the reported observations since it is the shape of the wave fronts that are required for interpretation and not their relative intensity.

On the optical images, one can observe the standing wave patterns between the incident and reflected wave by the photonic crystal mirror. In the case of the reference structure made of the PC flat mirror, flat interference fringes with a half-wavelength spatial periodicity are clearly resolved in the optical near-field images. Introduction of a defect in the planarity of the PC mirror surface, namely a bump, leads to a local deformation of the planarity of the standing wave pattern. More precisely, as clearly visible in the near-field measurements, a half-period shift of the fringes is measured locally above the bump on the mirror, which corresponds to a local phase shift of the reflected wave. As a consequence, cloaking the bump would result in suppressing this phase shift on the observed interference pattern. Experimentally, the near-field images recorded with the cloak structures reveal almost flat fringes in front of the cloak, which demonstrates that the bump has been properly cloaked. Since the contrast of these fringes remains the same as in the reference cases without cloak and since the reflectivity of the first row of the cloak pillars is low due to their subwavelength size, these flat fringes clearly result from the interference between the wave reflected by the photonic crystal mirror after passing through the cloak and the incident plane wave. Then, inside the cloak, as visible on all the presented images in Figs. 6 and 8, the measured optical near-field distributions are unfortunately highly modulated by the cloak topography [Fig. 8(a)], making us blind to the standing wave pattern inside it.

In addition, a quantitative measure of the cloaking efficiency can be derived from the evaluation of the modified Liao functional.[29] The fringes are defined as the lines corresponding to the maxima of the field intensity. Figure 7 shows these fringes for the three situations. According to the method of least squares, it is found that the deviations from a 15 μm segment are respectively 37, 129, and 52 for the flat mirror, the flat mirror with bump, and the cloaked structure (arbitrary unit is used). These raw data show that the measurements and the device's imperfections induce uncertainties which make the error bars very wide. However, when restricting the evaluation of the deviation to the 5 μm segment centered above the bump, the deviations become respectively 13, 76, and 16. In this case, it is found that the carpet leads to a reduction of the bump signature by a factor of 4.75, which is comparatively higher than the reduction factor of 3.7 obtained for a plasmonic carpet at 800 nm in Ref. 18.

As shown in Fig. 8, such experimental features, the strongly topographically modulated light inside the cloak as well as the standing wave with flat fringes showing the cloak efficiency, are observed all over the C band of telecommunication wavelengths, i.e., for wavelengths ranging from 1520 to 1580 nm. This wavelength range is limited experimentally at shorter wavelengths by the absorption of the InGaAs layer used for waveguiding and at longer wavelengths by our laser source.

V. NUMERICAL INVESTIGATION OF THREE-DIMENSIONAL FEATURES

In the experimental results in Figs. 6–8 the bump signature is at the same time more pronounced and less complex than the 2D numerical simulations from Fig. 6 would indicate. For instance, in Fig. 6(f) on both sides of the bump we can see a prominent "checkerboard" pattern due to the interference of waves reflected from the original PC surface and from the slanted sides of the bump. This pattern is expected to be absent from the experimental image, Fig. 6(e). To understand the origin of this difference, we have performed a series of numerical simulations of the 3D crystal that acts as a mirror. The crystal was assumed to be infinite and periodic in the x direction, but composed of only five unit cells (as in the experiment) in the y direction. It was illuminated with a quasicylindrical wave, which is a good approximation of the field generated by a subwavelength source (e.g., the outlet of a planar waveguide) located close to an air-dielectric interface at the distance of at least a few wavelengths from the observation point.[32] Specifically, the incident field had the form

$$\mathbf{E}_{\mathrm{inc}}(x,y,z) = (\hat{\mathbf{x}}\cos\alpha - \hat{\mathbf{y}}\sin\alpha) \times \exp[ik_0(x\sin\alpha + y\cos\alpha)]\mathcal{E}(z), \quad (1)$$

where

$$\mathcal{E}(z) = \begin{cases} 1 - ik_0\sqrt{\epsilon_{\mathrm{substrate}} - \epsilon_{\mathrm{air}}}z & \text{for } z > 0 \\ \exp(-ik_0\sqrt{\epsilon_{\mathrm{substrate}} - \epsilon_{\mathrm{air}}}z) & \text{for } z < 0, \end{cases} \quad (2)$$

α is the incidence angle, and k_0 the wave number in air. Here, the plane delimiting air-substrate interface is defined by $z = 0$, as in Fig. 2 (i.e., $z > 0$ corresponds to air and $z < 0$ to the

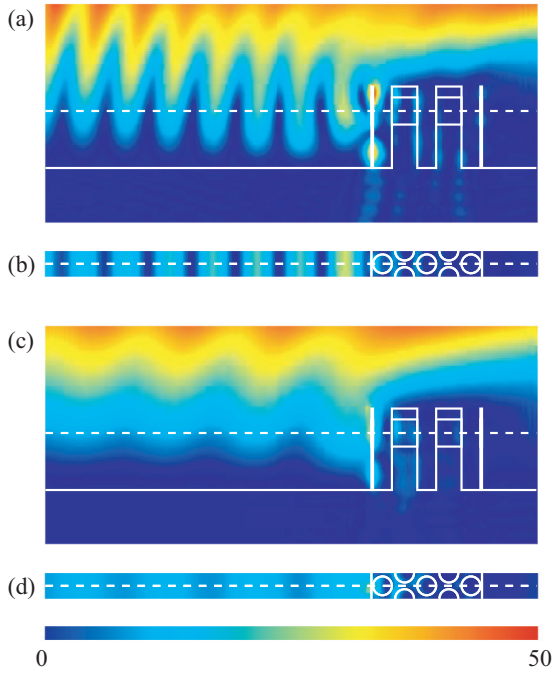

FIG. 9. (Color online) Magnitude of the electric field generated by a quasicylindrical wave incident on the PC mirror at the angle of (a), (b) $\theta = 0$ and (c), (d) $\theta = 60^\circ$. The panels (a) and (c) show vertical (yz) cross sections of the field along a plane bisecting the holes lying in the outermost rows; the panels (b) and (d) show horizontal (xy) cross sections of the field along the plane lying 1550 nm above the substrate and bisecting the guiding GaInAsP layer. The color scale is common for all panels. The plots were obtained in 3D finite-element simulations using GetDP (Ref. 34).

substrate). This equation is motivated by Eq. (14) from Ref. 33 and, physically, represents the field produced by a plane wave illuminating the air-substrate interface at a grazing angle. The full formula for a quasicylindrical wave [Eq. (12)][33] contains an additional decay factor $|y - y_{\text{source}}|^{-3/2}$, where y_{source} is the position of the source. We neglect this slowly varying factor, since we are only interested in the behavior of the incident field in a small range of y.

We consider two situations: The quasicylindrical wave launched in the direction normal to the surface of the crystal ($\theta = 0$) and at the angle $\theta = 60$ degrees with respect to that surface. The former case corresponds to wave scattering on the unmodified surface of the crystal and on the front surface of the bump; the latter, on the slanted sides of the bump. Figures 9(a), 9(b) and 9(c), 9(d) show the yz and xy cross sections of the total field produced in these two cases. Comparing the amplitude of the interference fringes in Figs. 9(b) and 9(d), we conclude that out-of-plane scattering at the crystal surface is much stronger at oblique than at normal incidence. In consequence, the slanted sides of the bump do not leave a strong mark on the interference pattern *in the incidence plane*, and the image collected by NSOM contains solely the fringes created by the interfaces perpendicular to the incident wave. In the NSOM image the signature of the bump appears clearly, since it results from the phase shift between the original crystal surface and the front side of the bump. Nevertheless, two-dimensional numerical simulations for the carpet cloak at oblique incidence do not provide satisfactory results, and a three-dimensional model for the entire structure (carpet and PC with bump) lies beyond our computational capabilities. Moreover, demonstration of cloaking at oblique incidence would require us to construct new samples. Consequently, we did not pursue any further the exploration of this carpet cloak.

The quality of the benchmark for the experimental validation of carpet cloaking relies on the good reflecting properties of the PC and the bump and could be improved by fabricating higher pillars, but this is sadly still out of reach. There is also the issue of cloaking at other incident angles. Here again, the fabricated PC with bump and carpet cloak is not optimal. In order to convince the reader that our design is a serious step towards a future realization of multiangle cloaking, we push further the complexity of the structure and study its efficiency in the next section.

VI. DESIGN OF A PHOTONIC CRYSTAL CARPET CLOAK FOR OBLIQUE INCIDENCE

We would like to investigate the design of a multi-incidence photonic crystal carpet cloak. Since we consider a PC with a complete stop band, we expect it will reflect most of p-polarized light at all angles. The challenge is to make a specially designed carpet such that the PC with a bump will reflect p-polarized light like a flat PC for all angles of incidence. To achieve this extra feature, we need to improve the design of the carpet cloak we tested experimentally at normal incidence. In order to better grasp the genuine difficulty to make such a carpet, we show in Fig. 10(a) the ideal

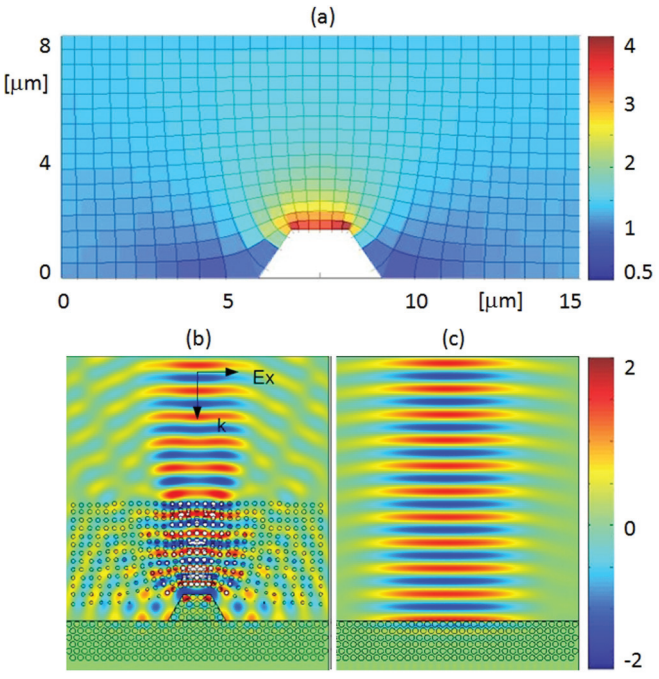

FIG. 10. (Color online) Design and numerical test of improved carpet at normal incidence: (a) Distribution of the relative permittivity and associated quasiconformal grid for the ideal carpet cloak; (b) real part of the magnetic field at 1540 nm for a normally incident Gaussian beam of waist 5 μm with amplitude set to unity on the metamaterial carpet dressing the bump on the PC; same plot for the PC on its own. White color is for values out of range.

distribution of the permittivity in the carpet, and the associated quasiconformal grid. A similar refractive index distribution for a different bump can be found in the paper by Li and Pendry.[11] We note that the relative permittivity should in principle take some values slightly lower than one near the PC.

However, with dielectric pillars in air, the lower bound for the effective refractive index is clearly greater than 1 (we use conventional effective medium theory here), hence we assume the regions whose refractive index should ideally be below 1 will simply be made of air. Such an approximation turns out to work fairly well. The optimal design is achieved through an optimization algorithm which consists of varying the radius of the pillars constituting the carpet within the range 74 to 151 nm. These pillars are placed at the nodes of a quasiconformal grid in order to mimic the refractive index averaged over the four cells surrounding each node of the quasiconformal grid as shown in Fig. 10(a). Some slight adjustments on the pillars' diameters are then made checking for each configuration the quality of cloaking (reduction of scattering by the bump). It is also not possible to achieve the highest values of the ideal refractive index with the dielectric pillars of permittivity 10.43 at hand near the bump [red color in Fig. 10(a)], as we want to place them at nodes of smaller cells.

The resulting design and accompanying numerical simulations for a Gaussian beam centered about the wavelength 1540 nm incident at an angle of 0 degrees (normal incidence) are shown in Fig. 10(b) (carpet dressing the PC with the bump) and in Fig. 10(c) (PC without bump) for comparison. One can see that the phase and amplitude of the magnetic field are comparable in panels (b) and (c), which demonstrates successful cloaking at normal incidence.

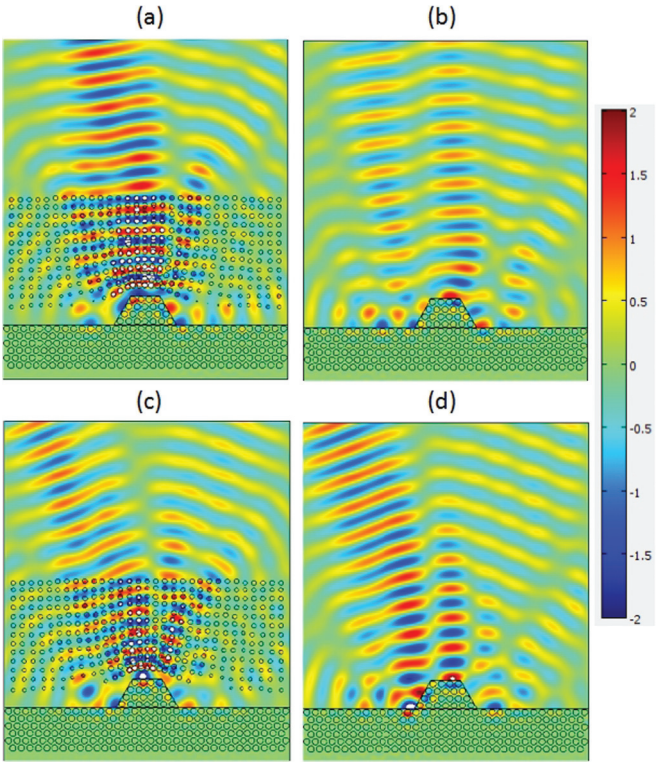

FIG. 11. (Color online) Numerical test of improved carpet at oblique incidence (small angle): Real part of the magnetic field at 1540 nm. (a) 10 degrees for a carpet and a bump; (b) 10 degrees for a bump; (c) 20 degrees for a carpet and a bump; (d) 20 degrees for a bump. The color bar corresponds to an incident Gaussian beam of waist 5 μm with amplitude set to unity (white color is for values out of range).

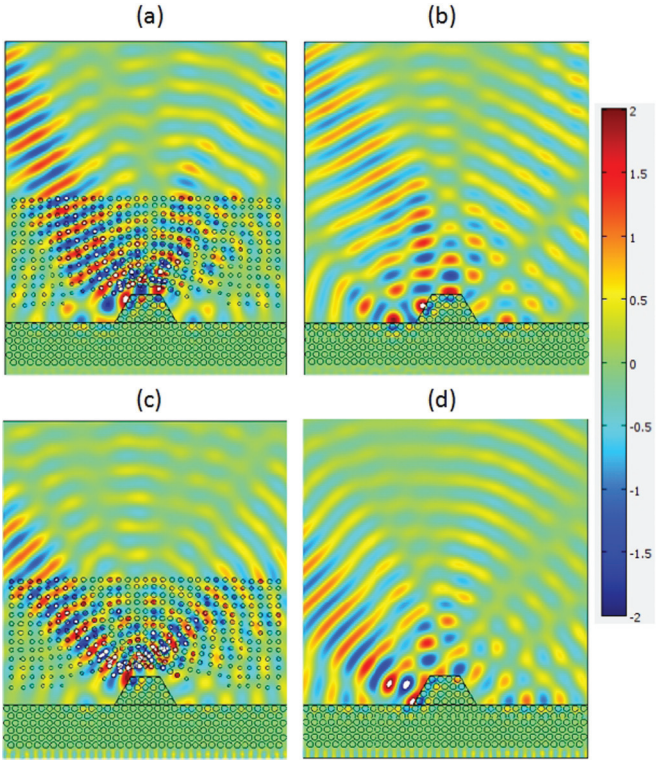

FIG. 12. (Color online) Numerical test of improved carpet at oblique incidence (large angle): real part of the magnetic field at 1540 nm. (a) 30 degrees for a carpet and a bump; (b) 30 degrees for a bump; (c) 45 degrees for a carpet and a bump; (d) 45 degrees for a bump. The color bar corresponds to an incident Gaussian beam of waist 5 μm with amplitude set to unity (white color is for values out of range).

Let us now investigate cloaking at other angles of incidence. We start with small angles of incidence, respectively 10 and 20 degrees in Figs. 11(a) and 11(b) [resp. (c) and (d)]. The reduced scattering when the cloak surrounds the bump is apparent in panels (a) and (c).

We further show in Fig. 12 numerical simulations for a Gaussian beam incident at 30 degrees and 45 degrees on a bump dressed with a carpet cloak, see panels (a) and (c). One can clearly see that the scattering is much reduced compared to the structure without the carpet, see panels (b) and (d).

Such an improved carpet cloak which works from normal incidence to oblique angles up to 45 degrees could be realized in the near future as the smallest features (pillar diameter of 74 nm and height of 2 μm) could be achieved with the processes described in this paper. The main challenge would be in fact the fabrication of pillars of varying radii, which requires an additional fabrication step. One would also like to have a larger aspect ratio to make the structure genuinely two dimensional (in order to greatly simplify the numerical modeling).

VII. CONCLUSION

In conclusion, a cloaking device with a photonic crystal mirror has been designed to operate at the telecommunication wavelength 1550 nm. This device has been fabricated using an original technique based on a novel one-mask process which makes it possible to create pillars and holes with an etching depth larger than 1.5 μm. The characterization of the cloaking structure has been performed with near-field measurements showing the interference fringes in the vicinity of the cloaking structure. The invisibility carpet is shown to operate efficiently for wavelengths ranging from 1520 to 1580 nm: The bump signature is reduced 4.75 times. The analysis of experimental results has been completed using three-dimensional calculations. Finally, we have proposed an improved carpet cloak working at oblique incidence and shown numerically its efficiency in the range of angles 0 to 45 degrees. However, this need be confirmed experimentally. We hope our work will foster efforts in this direction.

ACKNOWLEDGMENTS

This work was partly supported by the project FANI funded by the Agence Nationale de la Recherche (ANR). S.G. acknowledges funding from the European Union through ERC Starting Grant Anamorphism. G.S. would like to thank the Regional Council of Burgundy for financial support. Dr. Jensen Li is gratefully acknowledged for useful discussions.

[1] J. B. Pendry, D. Schurig, and D. R. Smith, Science **312**, 1780 (2006).
[2] U. Leonhardt, Science **312**, 1777 (2006).
[3] D. Van Dantzig, Proc. K. Ned. Akad. Wet. **37**, 521 (1934).
[4] D. Schurig, J. J. Mock, B. J. Justice, C. A. Cummer, J. B. Pendry, A. F. Starr, and D. R. Smith, Science **314**, 977 (2006).
[5] B. Kanté, D. Germain, and A. de Lustrac, Phys. Rev. B **80**, 201104 (2009).
[6] A. Greenleaf, M. Lassas, and G. Uhlmann, Math. Res. Lett. **10**, 685 (2003).
[7] U. Leonhardt and T. Tyc, Science **323**, 110 (2009).
[8] J. Percze, T. Tyc, and U. Leonhardt, New J. Phys. **13**, 083007 (2011).
[9] R. V. Kohn, H. Shen, M. S. Vogelius, and M. I. Weinstein, Inverse Probl. **24**, 015016 (2011).
[10] W. X. Jiang, T. J. Cui, X. M. Yang, Q. Cheng, R. Liu, and D. R. Smith, Appl. Phys. Lett. **92**, 264101 (2008).
[11] J. Li and J. B. Pendry, Phys. Rev. Lett. **101**, 203901 (2008).
[12] A. Cho, Science **329**, 277 (2010).
[13] R. Liu, C. Ji, J. J. Mock, J. Chin, T. J. Cui, and D. R. Smith, Science **323**, 366 (2008).
[14] J. H. Lee, J. Blair, V. A. Tamma, Q. Wu, S. J. Rhee, C. J. Summers, and W. Park, Opt. Express **17**, 12922 (2009).
[15] J. Valentine, J. Li, T. Zentgraf, G. Bartal, and X. Zhang, Nat. Mater. **8**, 569 (2009).
[16] L. H. Gabrielli, J. Cardenas, C. B. Poitras, and M. Lipson, Nat. Photon. **8**, 461 (2009).
[17] N. Ergin, T. Stenger, P. Brenner, J. B. Pendry, and M. Wegener, Science **328**, 337 (2010).
[18] J. Renger, M. Kadic, G. Dupont, S. S. Aćimović, S. Guenneau, R. Quidant, and S. Enoch, Opt. Express **18**, 15757 (2010).
[19] X. Chen, Y. Luo, J. Zhang, K. Jiang, J. B. Pendry, and S. Zhang, Nat. Commun. **2**, 176 (2011).
[20] E. Schonbrun, Q. Wu, W. Park, T. Yamashita, C. J. Summers, M. Abashin, and Y. Fainman, Appl. Phys. Lett. **90**, 041113 (2007).
[21] F. Zolla, S. Guenneau, A. Nicolet, and J. B. Pendry, Opt. Lett. **32**, 1069 (2007).
[22] W. Śmigaj, B. Gralak, R. Pierre, and G. Tayeb, Opt. Lett. **34**, 3532 (2009).
[23] G. Scherrer, M. Hofman, W. Śmigaj, B. Gralak, X. Mlique, O. Vanbsien, D. Lippens, C. Dumas, B. Cluzel, and F. de Fornel, Appl. Phys. Lett. **97**, 071119 (2010).
[24] W. Śmigaj and B. Gralak, Phys. Rev. B **85**, 035114 (2012).
[25] H. Kosaka, T. Kawashima, A. Tomita, M. Notomi, T. Tamamura, T. Sato, and S. Kawakami, Phys. Rev. B **58**, R10096 (1998).
[26] S. Enoch, G. Tayeb, and B. Gralak, IEEE Trans. Antennas Propag. **51**, R2659 (2003).
[27] N. Fabre, L. Lalouat, B. Cluzel, X. Mélique, D. Lippens, F. de Fornel, and O. Vanbésien, Phys. Rev. Lett. **101**, 073901 (2008).
[28] P. Zhang, Y. Jin, and S. He, Opt. Express **16**, 3161 (2008).
[29] G. Liao and H. Liu, Num. Math. PDEs **9**, 261 (1993).
[30] Z. Liang and J. Li, Opt. Express **19**, 16821 (2011).
[31] N. Fabre, S. Fasquel, C. Legrand, X. Mélique, M. Muller, M. François, O. Vanbésien, and D. Lippens, Opto-Electron. Rev. **14**, 225 (2006).
[32] C. H. Gan, L. Lalouat, P. Lalanne, and L. Aigouy, Phys. Rev. B **83**, 085422 (2011).
[33] P. Lalanne, J. P. Hugonin, H. T. Liu, and B. Wang, Surf. Sci. Rep. **64**, 453 (2009).
[34] P. Dular, C. Geuzaine, F. Henrotte, and W. Legros, IEEE Trans. Magn. **34**, 3395 (1998).